ELSEVIER

Chemical Engineering Science 61 (2006) 4490–4502

Chemical Engineering Science

www.elsevier.com/locate/ces

Modelling the flow of power-law fluids through anisotropic porous media at low-pore Reynolds number

L. Orgéas[a,*], Z. Idris[a], C. Geindreau[a], J.-F. Bloch[b], J.-L. Auriault[a]

[a]*Laboratoire Sols-Solides-Structures (3S), CNRS-Universités de Grenoble (INPG-UJF), BP 53, 38041 Grenoble Cedex, France*
[b]*Laboratoire de Génie des Procédés Papetiers (LG2P), Ecole Française de Papeterie de Grenoble-Institut National Polytechnique de Grenoble, 38000 Grenoble Cedex, France*

Received 9 September 2005; received in revised form 23 January 2006; accepted 31 January 2006
Available online 5 May 2006

Abstract

The flow of power-law fluids through fibrous media at low-pore Reynolds number is investigated using the homogenization method for periodic structures with multiple scale expansions. This upscaling process shows that the macroscopic pressure gradient is also a power-law of the volume averaged velocity field. To determine the complete structure of the macroscopic flow law, numerical simulations have to be performed on representative elementary volume of porous media. In this paper, this has been achieved on 2D periodic arrays of parallel fibers with elliptical cross section of different aspect ratios. It is found that macroscopic flow models already proposed in the literature fail in reproducing numerical data within the whole volume fractions of fibers and aspect ratios ranges. Consequently, a novel methodology is proposed to establish the macroscopic tensorial seepage law within the framework of the theory of anisotropic tensor functions and using mechanical iso-dissipation curves. This methodology is illustrated through our numerical results.

Keywords: Porous media; Fibrous media; Non-Newtonian fluids; Mathematical modelling and simulation; Filtration; Anisotropy

1. Introduction

Many processes in polymer composites, textiles, papers, oil, food, cosmetic and pharmaceutical industries involve the flow of non-Newtonian fluids through anisotropic porous media. In order to control and optimize such processes, suitable tensorial flow laws are required. When the local Reynolds number is small, i.e., in the creeping flow regime, lots of theoretical, experimental and numerical works have been conducted in the case of Newtonian flowing fluids and isotropic, or anisotropic porous media. They lead to tensorial forms of the linear 1D Darcy law (Darcy, 1856; Jackson and James, 1986; Advani et al., 1994). Efforts are now focusing on the determination of the permeability tensor in real porous or fibrous microstructures (Clague and Philips, 1997; Koponen et al., 1998; Song et al., 2004; Bernard et al., 2005). Due to coupling effects between the microstructure of porous media and the rheology of the fluid, the extension of the Darcy law in the case of non-Newtonian fluids is complex, even in the creeping flow regime. Among the numerous works dedicated to this problem (see the review of Chhabra et al., 2001), most of them have dealt with power-law flowing fluids, which is the simplest way to account for purely viscous and non-Newtonian effects of complex liquids. Resulting macroscopic models are usually restricted to "simple" porous or fibrous media. Furthermore, they consist in 1D modified version of the Darcy law. The anisotropy of many natural or manufactured porous media and the consequence on the macroscopic flow law are rarely studied (Fadili et al., 2002). Consequently, tensorial anisotropic models are scarce.

More recent works have analyzed numerically the anisotropy of the steady transverse slow flow of power-law fluids through square or triangular arrays of aligned fibers with circular (Spelt et al., 2001; Idris et al., 2004) and elliptic (Woods et al., 2003) cross sections. These works are based on numerical results deduced from direct simulation (Spelt et al., 2001; Woods et al., 2003) or specific boundary value problems arising from an

* Corresponding author. Tel.: +33 476 827 073; fax: +33 476 827 043.
E-mail address: Laurent.Orgeas@hmg.inpg.fr (L. Orgéas).

0009-2509/$ - see front matter © 2006 Elsevier Ltd. All rights reserved.
doi:10.1016/j.ces.2006.01.046

upscaling process (Idris et al., 2004). Within large volume fractions of fibers and power-law exponents ranges, it was shown that the flow of power-law fluid in the symmetry axes of the microstructure could be deduced as a good approximation from that of a Newtonian fluid in the same situation, as already suggested by Bruschke and Advani (1993). The dependence between the rheology of the fluid, the anisotropies of the microstructure and of the seepage law were also clearly underlined. For example, when the cross section of the fibers is circular and for square and triangular arrangements, the transverse seepage law display isotropy with Newtonian fluids (due to both the particular symmetries of the studied microstructures and the linearity of the physics), whereas it is found to be anisotropic with power-law fluids (Idris et al., 2004). Woods et al. (2003) have proposed the first and only (to our knowledge) macroscopic anisotropic model for power-law fluids flows through porous media from their numerical results. Unfortunately, the proposed model is not written in a intrinsic form, i.e., in a tensorial form: its expression in a reference frame different from the one they used is not straightforward. Moreover, as the model is based on lubrication-like assumptions, its domain of validity is restricted to microstructures with high volume fraction of fibers. Indeed, Idris et al. (2004) have shown, in the case of fibers with circular cross section at mild or low volume fraction of fibers, that the macroscopic model proposed by Woods et al. (2003) fails in describing numerical results deduced from simulation at the local scale. Finally, the application of the model to other types of porous microstructures is not evident.

Thereby, the aim of the present paper is to pursue the work of Woods et al. (2003), proposing a novel theoretical framework to build macroscopic tensorial flow law of power-law fluids through anisotropic porous media. Recently, the structure and the properties of the macroscopic flow law have been derived from the fluid flow description at the pore scale by using the homogenization method for periodic structures using multiple scale expansions (Shah and Yortsos, 1995; Bourgeat and Mikelic, 1996; Auriault et al., 2002): the main assumptions related to the method, the physics studied at the fiber scale as well as the principal theoretical results deduced from the upscaling are briefly recalled in Section 2. The transverse flow of power-law fluids through square array of parallel fibers with elliptical cross section is then studied numerically at the fiber scale in Section 3. The limitation of the model of Woods et al. (2003) is pointed out. In order to overcome this, a general framework based on the theory of anisotropic tensor functions is then presented in Section 4 to formulate the macroscopic flow law of power-law fluids through orthotropic fibrous media. A new model is proposed within this framework and using mechanical iso-dissipation curves. Constitutive parameters of the so-derived model are then deduced from numerical results presented in Section 3. Let us remark that the choice of the microstructure is used in this paper has been done in order (i) to compare our results with data and predictions of models available in the literature, (ii) to check the improvements brought by the new proposal. However, the methodology proposed is applicable to more complex porous microstructures.

2. Theoretical upscaling

In a previous work (Auriault et al., 2002), the flow law for a power-law fluid in porous media was upscaled using the homogenization method for periodic structures with multiple scale expansions (Bensoussan et al., 1978; Sanchez-Palencia, 1980; Auriault, 1991). This deterministic theoretical technique allows to establish the general form of the flow law and its domain of validity, (i) starting from the description of physics at the scale of the fibers, (ii) assuming the periodicity of the considered porous medium and the physical fields (iii) when the condition of scale separation is fulfilled. The separation of scale is written $\varepsilon = l_c/L_c$, where l_c and L_c are the characteristic lengths of the representative elementary volume and the macroscopic sample or excitation, respectively. In the following subsections, we briefly recall the theoretical reasoning and the main results obtained in Auriault et al. (2002): the reader is referred to this reference for details about the theoretical aspects of the upscaling.

2.1. Fluid flow description at the pore scale

The REV of the considered local problem is a periodic porous microstructure of total volume Ω_{rev}, the rigid solid phase (fibers in this work) occupying a volume Ω_s. The porous medium is saturated by a fluid which occupies a volume Ω_l. The fluid is supposed to be incompressible and purely viscous. Its viscosity μ is assumed to be a power-law function of the microscopic shear strain rate $\dot{\gamma}$:

$$\mu = \mu_0 \dot{\gamma}^{n-1}, \quad \dot{\gamma} = \sqrt{2\mathbf{D} : \mathbf{D}}, \tag{1}$$

where μ_0 is the shear consistency of the fluid, $\mathbf{D}$ is the strain rate tensor defined as a function of the local velocity field $\mathbf{v}$, and where the power-law exponent n characterizes the strain rate sensitivity of the fluid. At the pore scale, the mass and momentum balances for an isothermal steady slow flow (inertial effects are neglected) of such a power-law fluid are, respectively,

$$\left.\begin{aligned} &\nabla \cdot \mathbf{v} = 0 \\ &\nabla p = 2\mu_0 \nabla \cdot (\dot{\gamma}^{n-1}\mathbf{D}) \end{aligned}\right\} \quad \text{in } \Omega_l. \tag{2}$$

where the differential operator ∇ is calculated with respect to the physical variable $\mathbf{X}$. The fluid flow description at the fiber scale is completed by a no-slip condition on the fluid–solid interface Γ:

$$\mathbf{v} = \mathbf{0} \quad \text{on } \Gamma. \tag{3}$$

2.2. Dimensional analysis

Using l_c as the characteristic length, it can be shown (Auriault et al., 2002; Idris et al., 2004) that the dimensionless form of (2–3) introduces a dimensionless number Q:

$$Q = \frac{\Delta p_c}{\mu_0}\left(\frac{l_c}{v_c}\right)^n. \tag{4}$$

If now we consider a filtration experiment performed with a porous sample of length L_c, the characteristic macroscopic pressure gradient $\Delta p_c/L_c$ is balanced by volumetric viscous drag forces of characteristic value f_c induced by the local shearing of the fluid at a characteristic shear rate v_c/l_c (v_c is a local characteristic velocity), i.e.:

$$\frac{\Delta p_c}{L_c} = f_c = \mathcal{O}\left(\frac{\mu_0}{l_c}\left(\frac{v_c}{l_c}\right)^n\right). \tag{5}$$

According to (5), the order of magnitude of Q must be equal to ε^{-1} (Auriault, 1991).

2.3. Asymptotic analysis

By following the technique of multiple scale expansions (Bensoussan et al., 1978; Sanchez-Palencia, 1980; Auriault, 1991), the velocity $\mathbf{v}$ and the pressure p are looked for in the form of asymptotic expansions of powers of ε,

$$\begin{cases} \mathbf{v} = \mathbf{v}^{(0)}(\mathbf{x},\mathbf{y}) + \varepsilon\mathbf{v}^{(1)}(\mathbf{x},\mathbf{y}) + \cdots, \\ p = p^{(0)}(\mathbf{x},\mathbf{y}) + \varepsilon p^{(1)}(\mathbf{x},\mathbf{y}) + \cdots, \end{cases} \tag{6}$$

where the dimensionless macroscopic space variable $\mathbf{x}=\mathbf{X}/L$ is related to the dimensionless microscopic space variable $\mathbf{y}=\mathbf{X}/l$ by $\mathbf{x} = \varepsilon\mathbf{y}$ and where the $p^{(i)}$ and $\mathbf{v}^{(i)}$ are periodic on the REV. Substituting these expansions in the dimensionless form of the set (2–3) gives, by identification of the like powers of ε, successive boundary value problems to be investigated.

2.4. Macroscopic description

It can be shown by the homogenization process: (i) that the first order pressure $p^{(0)}$ is constant over the REV and (ii) that the macroscopic mass and momentum balance equations of the macroscopic equivalent medium are, respectively,

$$\begin{cases} \nabla\cdot\langle\mathbf{v}^{(0)}\rangle = 0, \\ \nabla p^{(0)} = \mathbf{f}(\langle\mathbf{v}^{(0)}\rangle, \mu_0, n, \text{microstructure}), \end{cases} \tag{7}$$

where

$$\langle\mathbf{v}^{(0)}\rangle = \frac{1}{\Omega_{\text{rev}}}\int_{\Omega_l}\mathbf{v}^{(0)}\,\mathrm{d}V \tag{8}$$

is the volume averaged velocity field at the first order, and where $\mathbf{f}$ can be seen as a volumetric viscous drag force. It can be proved that $\mathbf{f}$ is a homogeneous function of degree n of the volume averaged velocity field $\langle\mathbf{v}^{(0)}\rangle$:

$$\forall\xi\in\mathbb{R}^+, \quad \mathbf{f}(\xi\langle\mathbf{v}^{(0)}\rangle) = \xi^n\mathbf{f}(\langle\mathbf{v}^{(0)}\rangle). \tag{9}$$

As pointed out in Auriault et al. (2002), (7b) can be put in a reverse form, i.e., $\langle\mathbf{v}^{(0)}\rangle = \mathbf{g}(\nabla p^{(0)}, \mu_0, n, \text{microstructure})$, where $\mathbf{g}$ is an homogeneous function of degree $1/n$ of $\nabla p^{(0)}$. When $\mathbf{g}$ is introduced in (7a), a complete boundary value problem is obtained at the macroscale in terms of $p^{(0)}$. In Section 4, expressions of $\mathbf{f}$ (or $\mathbf{g}$) are proposed in the case of orthotropic porous media.

3. Computational filtration experiments

3.1. Studied microstructures and fluids

In order to highlight the influence of the fibrous microstructure on the macroscopic flow law, i.e., the constitutive relation $\mathbf{f}(\mu_0, n, \langle\mathbf{v}^{(0)}\rangle, \text{microstructure})$, the flow of a power-law fluid across a square array of infinite, parallel and identical fibers of elliptical cross section is considered. For a sake of simplicity, only the flow perpendicular to the fibers is studied, reducing the problem to a 2D analysis: as shown in Fig. 1, numerical simulation is performed with 2D periodic arrays of elliptical inclusions of aspect ratio $r=b/a$, a and b being their radius in the major $\mathbf{e}_\text{I}$ and minor $\mathbf{e}_\text{II}$ axes, respectively. The sizes of the periodic REV are l and rl, the volume fraction of fibers $c=\pi ab/rl^2=\pi a^2/l^2$ ranges from 0 to $c_{\max}=\pi/4$. When $r\neq 1$, the microstructures display two material symmetry axes (dashed-dotted lines in Fig. 1): $\mathbf{e}_\text{I}$, $\mathbf{e}_\text{II}$, so that they are orthotropic. When $r=1$, they are tetratropic: two extra symmetry axes must be taken into account, i.e., $\mathbf{e}_\text{I}+\mathbf{e}_\text{II}$ and $\mathbf{e}_\text{I}-\mathbf{e}_\text{II}$ (Idris et al., 2004). In this work, the axes $\mathbf{e}_\text{I}$ and $\mathbf{e}_\text{II}$ of the microstructures have been chosen to be respectively equal to the reference frame axes $\mathbf{e}_1$ and $\mathbf{e}_2$ (see Fig. 1). Finally, the flow was investigated with the following microstructural and rheological parameters: $l=1$ m, $c\in[0.01; c_{\max}-0.01]$, $r\in[0.2;5]$, $\mu_0=1\,\text{Pa}\,\text{s}^{-n}$ and $n\in[0.3;1.5]$.

Notice that these microstructures are identical to those used in previous numerical works (for $r=1$, Sangani and Yao, 1988; Edwards et al., 1990; Berdichevsky and Cai, 1993; Bruschke and Advani, 1993; Spelt et al., 2001; Idris et al., 2004, and for $r\neq 1$, Woods et al., 2003). They are also close to those studied in previous numerical works based on cell-type boundary conditions (see, for examples Epstein and Masliyah, 1972 when $r\neq 1$ and $n=1$, and Vijaysri et al., 1999 when $r=1$ and $n\neq 1$).

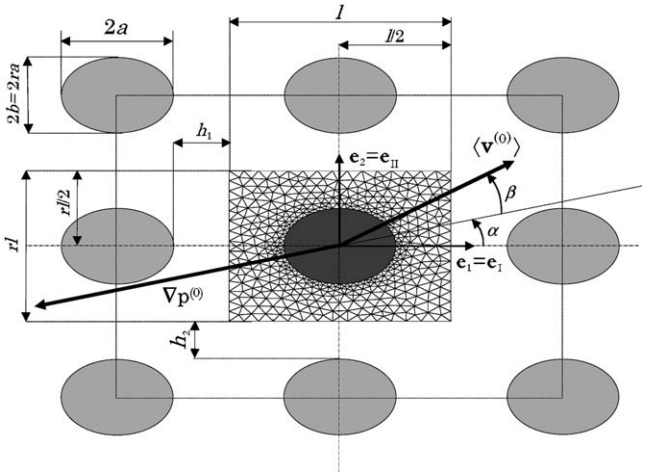

Fig. 1. Square array of elliptical solid inclusions. The periodic representative elementary volume (REV) of such a microstructure is given by the centered P2–P1 finite element mesh.

3.2. Numerical procedure

In order to study the macroscopic flow law, the viscous drag force $\mathbf{f}$ must be expressed as a function of the volume averaged velocity $\langle \mathbf{v}^{(0)} \rangle$. For that purpose, one must first determine the values of $\mathbf{v}^{(0)}$ in the whole REV. It can be rigorously shown from the upscaling procedure (Auriault et al., 2002) that $\mathbf{v}^{(0)}$ is the solution in the REV of the following well-posed dimensional boundary values problem:

$$\begin{cases} \nabla \cdot \mathbf{v}^{(0)} = 0 & \text{in } \Omega_l, \\ \nabla p^{(0)} + \nabla \varepsilon p^{(1)} = 2\mu_0 \nabla \cdot (\dot{\gamma}^{(0)^{n-1}} \mathbf{D}^{(0)}) & \text{in } \Omega_l, \\ \mathbf{v}^{(0)} = \mathbf{0} & \text{on } \Gamma, \end{cases} \tag{10}$$

where the unknowns $\mathbf{v}^{(0)}$ and $\varepsilon p^{(1)}$ are periodic, and where the macroscopic pressure gradient $\nabla p^{(0)}$ is given on the entire REV. As in Idris et al. (2004), this boundary values problem was solved using the software Femlab® (Femlab, 2004) with a mixed pressure–velocity (P1–P2) finite element formulation (see Fig. 1 for a typical mesh used to run the simulation). Hence, the microstructures are submitted to a macroscopic pressure gradient $\nabla p^{(0)}$ of intensity denoted $\|\nabla p^{(0)}\|$ such that (see Fig. 1)

$$\nabla p^{(0)} = -\|\nabla p^{(0)}\|(\cos\alpha \mathbf{e}_1 + \sin\alpha \mathbf{e}_2), \tag{11}$$

where $\alpha = (\mathbf{e}_1, \widehat{-\nabla p^{(0)}})$. The resulting macroscopic velocity $\langle \mathbf{v}^{(0)} \rangle$ of intensity $\|\langle \mathbf{v}^{(0)} \rangle\|$ is such that

$$\begin{aligned} \langle \mathbf{v}^{(0)} \rangle &= \|\langle \mathbf{v}^{(0)} \rangle\|(\cos(\alpha+\beta)\mathbf{e}_1 + \sin(\alpha+\beta)\mathbf{e}_2) \\ &= u\mathbf{e}_1 + v\mathbf{e}_2, \end{aligned} \tag{12}$$

where $\beta = (\widehat{-\nabla p^{(0)}}, \langle \mathbf{v}^{(0)} \rangle)$ (see Fig. 1).

3.3. Numerical results: on-axis flows

The flow along the $\mathbf{e}_1$ axis ($\alpha = 0$) is first studied. Due to the symmetry of the microstructure (Idris et al., 2004), it was systematically found that $\beta = 0$. Likewise, in this particular case, the flow law in $(\mathbf{e}_1, \mathbf{e}_2)$ can be put in the classical form (Bruschke and Advani, 1993; Spelt et al., 2001; Woods et al., 2003)

$$f_1 = \frac{\partial p^{(0)}}{\partial X_1} = -n_d \frac{\pi}{c} \frac{\mu_0}{a^{n-1} k_1^*(c,n,r)} |u|^{n-1} u, \tag{13}$$

where n_d is the number of cylinders per unit of cross area ($n_d = 1/rl^2$ in this work), k_1^* is a dimensionless rheological function that depends on the volume fraction of fibers c, the power-law exponent n and on the aspect ratio r. When $n=1$, it can be shown from (13) that $ra^2k_1^*$ represents the first principal component of the permeability tensor. Fig. 2 shows the evolution of k_1^* with the volume fraction of fibers c for different values of n and r:

- k_1^* is a decreasing function of c, tends towards infinite when $c \to 0$ and 0 when $c \to c_{\max}$,
- the role of the microstructure is also revealed by the aspect ratio r: the higher the aspect ratio, the higher the thickness

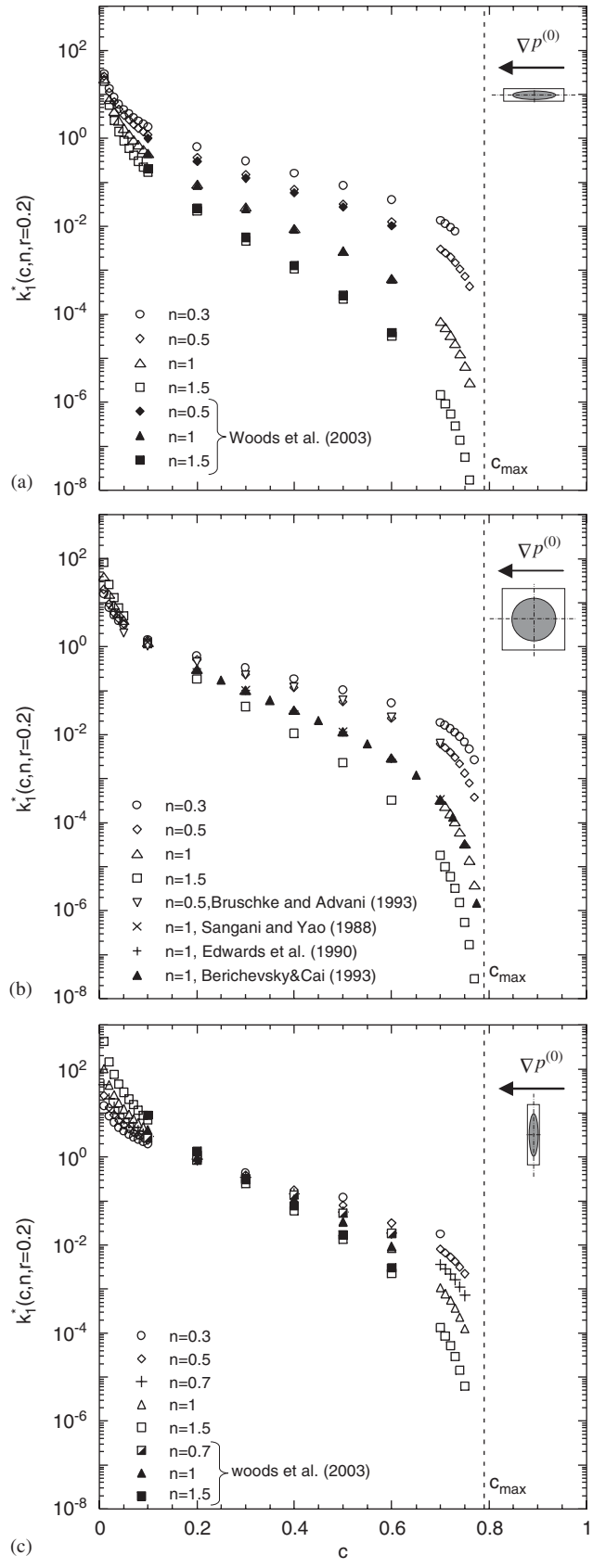

Fig. 2. Evolution of $k_1^*(c,n,r)$ with the volume fraction of fibers c for various aspect ratios, i.e., $r = 0.2$ (a), $r = 1$ (b) and $r = 5$ (c) and for various power-law exponents.

$2h_2$ between two adjacent vertical fibers (cf. Fig. 1), and the higher the value of k_1^*,
- the increase of the power-law exponent n, i.e., from shear thinning to shear thickening fluids, yields also to an increase of k_1^* at high volume fractions of fiber, this trend being reversed at low fiber content,
- numerical results coming from the literature for identical microstructures have also been plotted in the figure: the present results show a good correlation with them.

As already underlined by Woods et al. (2003), the flow along the $\mathbf{e}_2$ axis ($\alpha=\pi/2$) for those particular orthotropic microstructures, which is characterized by

$$f_2 = \frac{\partial p^{(0)}}{\partial X_2} = -n_d \frac{\pi}{c} \frac{\mu_0}{a^{n-1} k_2^*(c,n,r)} |v|^{n-1} v \tag{14}$$

is entirely known from the knowledge of $k_1^*(c,n,r)$, since the symmetries of the microstructures yield:

$$k_2^*(c,n,r) = r^{n-1} k_1^*(c,n,r^{-1}). \tag{15}$$

The 1D-flow law can (13) involve the rheological function k_1^*, that could be approximated by analytical cell, lubrication or hybrid models developed for those kind of fibrous microstructures and for Newtonian (Happel, 1959; Kuwabara, 1959; Keller, 1964) or power-law fluids (Bruschke and Advani, 1993; Woods et al., 2003). Nonetheless, the physical meaning of k_1^* is not evident in the case of power-law fluids. Instead of (13), another simple 1D-flow law can be built with the help of the order of magnitude expression (5). For that purpose the characteristic velocity v_c and length l_c related to the microstructure and the local flow must be evaluated. When the flow is along $\mathbf{e}_1$ axis, it seems reasonable to assume that l_c is linked to half the gap between two neighboring vertical fibers h_2 (see Fig. 1). Thus, we have

$$l_c = \lambda_1 h_2 = \lambda_1 r a \left(\frac{1-\sqrt{\Phi}}{\sqrt{\Phi}} \right), \tag{16}$$

where $\Phi=c/c_{\max}$ and λ_1 a rheological function that can depend on c, n and r. Using a simple mass balance argument, the characteristic velocity v_c associated with l_c can be written as

$$v_c = \frac{rl}{l_c} u = \frac{rl}{\lambda_1 h_2} u = \frac{1}{\lambda_1 (1-\sqrt{\Phi})} u. \tag{17}$$

Consequently, from (5), (16) and (17) it becomes

$$f_1 = -\frac{\mu_0}{(\lambda_1(1-\sqrt{\Phi}))^{2n+1}} \left(\frac{\sqrt{\Phi}}{ra} \right)^{n+1} |u|^{n-1} u. \tag{18}$$

Similarly, the flow along the $\mathbf{e}_2$ axis is expressed as

$$f_2 = -\frac{\mu_0}{(\lambda_2(1-\sqrt{\Phi}))^{2n+1}} \left(\frac{\sqrt{\Phi}}{a} \right)^{n+1} |v|^{n-1} v \tag{19}$$

choosing in this case $l_c = \lambda_2 h_1$. Note that the symmetries of the studied microstructures allow to write

$$\lambda_2(c,n,r) = \lambda_1(c,n,r^{-1}). \tag{20}$$

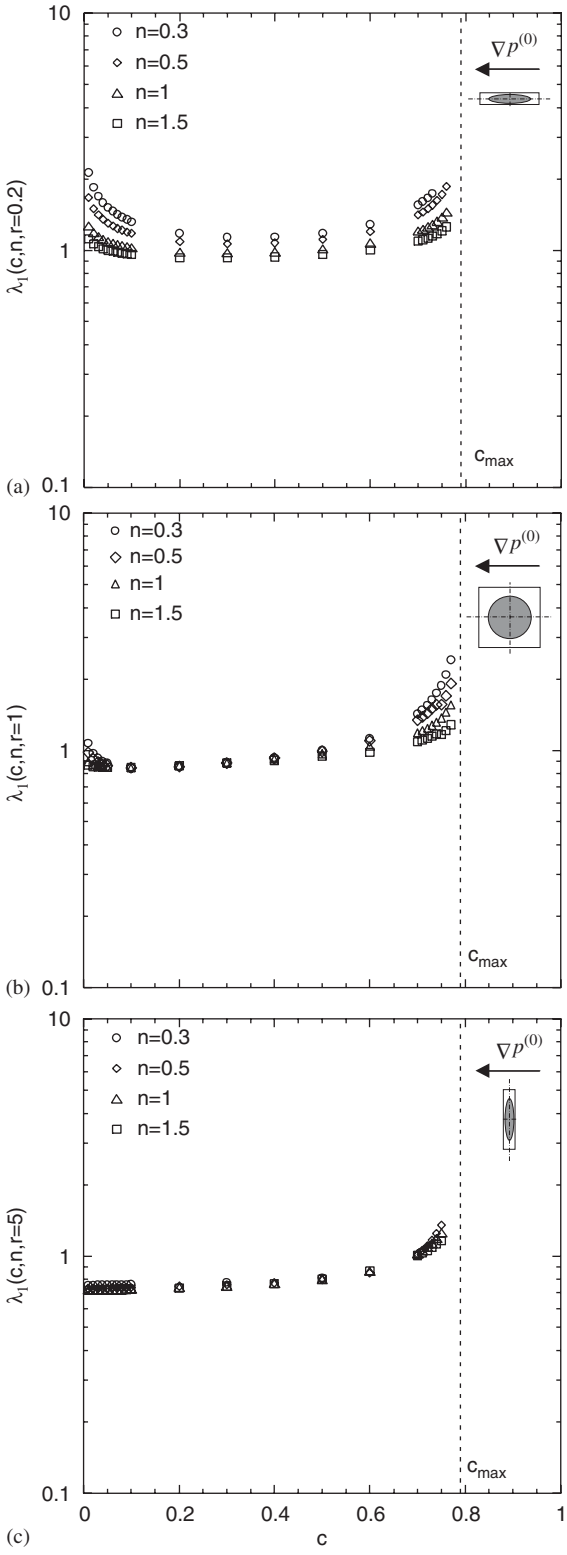

Fig. 3. Evolution of $\lambda_1^*(c,n,r)$ with the volume fraction of fibers c for various aspect ratios, i.e., $r=0.2$ (a), $r=1$ (b) and $r=5$ (c) and for various power-law exponents.

The evolution of λ_1 as a function of c is plotted in Fig. 3 for various values of r and n. This figure shows that the values of λ_1 are not constant within the investigated values of

c, n, and r, but are $\mathcal{O}(1)$. Thus, with the macroscopic flow law (18), the respective roles of the fiber mean radius a and aspect ratio r, the power-law exponent n and the normalized fiber content Φ on the drag force f_1 are more emphasized in respect to expression (13). In the following, a similar simple reasoning will be used in order to build the tensorial flow law (cf. Section 4.3).

3.4. Numerical results: off-axis flow

To further highlight the anisotropy of the flow law, numerical simulations are also carried out by imposing a macroscopic pressure gradient $\nabla p^{(0)}$ of the same intensity $\|\nabla p^{(0)}\|$ but with an angle $0 \leqslant \alpha \leqslant \pi$. Figs. 4 and 5 show, respectively, the evolutions of the computed values of $\|\langle \boldsymbol{v}^{(0)} \rangle(\alpha)\| / \|\langle \boldsymbol{v}^{(0)} \rangle(0)\|$ and β as functions of α, for various volume fraction of fibers, power-law exponents and aspect ratios. Due to the symmetries of the REVs, the curves are only plotted for $0 \leqslant \alpha \leqslant \pi/4$ and $0 \leqslant \alpha \leqslant \pi/2$ for $r = 1$ and $r \neq 1$, respectively. As in Idris et al. (2004), these figures conjure up the following comments:

- In general, the macroscopic velocity field is not aligned with the macroscopic pressure gradient, except when $\alpha = \kappa\pi/\tau$ (κ being an integer, $\tau = 4$ if $r = 1$ or 2 if $r \neq 1$), i.e., when the pressure gradient is parallel to the symmetry axes: the flow law displays tetratropy when $r = 1$ and orthotropy in other situations.
- When $n = 1$ and $r = 1$, the macroscopic velocity $\langle \boldsymbol{v}^{(0)} \rangle$ is always aligned with $\nabla p^{(0)}$ ($\beta = 0, \forall \alpha$) and its norm is constant: these numerical results, that are induced by the linearity of the problem in this situation, show that the transverse macroscopic flow law is isotropic, even if the fibrous microstructures display tetratropy.
- The coupling between the fluid rheology and the microstructure is complex.
  - For instance, the signs of the deviations $\Delta\beta(\alpha) = \beta(\alpha) - \beta(0)$ and $\Delta\|\langle \boldsymbol{v}^{(0)} \rangle\|$ for shear thinning ($n < 1$) or shear thickening ($n > 1$) fluids are different, sometimes with opposite signs (see Figs. 5(a,d,g) and 4(a,d,g) for example).
  - For Newtonian and shear thickening fluids, the anisotropy is less and less pronounced as the volume fraction of fibers diminishes or the cross section of fiber becomes circular: $|\Delta\beta|_{\max}$, $\Delta\|\langle \boldsymbol{v}^{(0)} \rangle\|_{\max}$ diminish as $c \to 0$ or $r \to 1$. Nevertheless, this trend breaks down for shear thinning fluids and $r \neq 1$: as shown in Fig. 4(b and c) (d–f) (h and i), $\Delta\|\langle \boldsymbol{v}^{(0)} \rangle\|_{\max}$ is maximal at mild fiber content (Fig. 4(d–f)).

4. Macroscopic modelling

4.1. General form of the macroscopic law

From the numerical results presented in the previous section, the form of the macroscopic viscous drag force $\mathbf{f}$ is now studied. We have shown previously that the macroscopic response exhibited orthotropy or higher order symmetries (tetra or isotropy). Therefore, we will restrict the presentation to orthotropic flow models (or with higher number of symmetries). For general anisotropy, the readers are referred to the guidelines given in Auriault et al. (2002).

If the microstructure displays orthotropy, i.e., with three orthogonal symmetry planes of normal $\mathbf{e}_i$ ($i = \mathrm{I}, \mathrm{II}, \mathrm{III}$), it can be shown from the theory of anisotropic tensor functions (Smith, 1971; Boehler, 1978, 1979; Boelher, 1987; Liu, 1982) that the microstructure tensors

$$\mathbf{M}_i = \mathbf{e}_i \otimes \mathbf{e}_i, \quad i = \mathrm{I}, \mathrm{II}, \mathrm{III} \tag{21}$$

have to be taken into account in the formulation of $\mathbf{f}$. More precisely, $\mathbf{f}$ can be expressed as

$$\mathbf{f} = -(\varphi_{\mathrm{I}}\mathbf{M}_{\mathrm{I}} + \varphi_{\mathrm{II}}\mathbf{M}_{\mathrm{II}} + \varphi_{\mathrm{III}}\mathbf{M}_{\mathrm{III}}) \cdot \langle \mathbf{v}^{(0)} \rangle, \tag{22}$$

where the scalar rheological functions φ_i depend on the geometry of the porous medium, μ_0 and n, and are, in accordance with property (9), homogeneous functions of degree $(n-1)$ of the velocity invariants I_i defined as

$$I_i = \sqrt{\langle \mathbf{v}^{(0)} \rangle \cdot \mathbf{M}_i \cdot \langle \mathbf{v}^{(0)} \rangle}, \quad i = \mathrm{I}, \mathrm{II}. \tag{23}$$

The following subsections detail possible expressions of the functions φ_i.

4.2. The model of Woods et al. (2003)

Macroscopic tensorial flow laws through anisotropic fibrous media are very scarce. To our knowledge, the only proposal was given by Woods et al. (2003) for transverse flow of power-law fluids through the fibrous microstructures sketched in Fig. 1. This 2D-law has been expressed in the reference frame $(\mathbf{e}_1, \mathbf{e}_2) = (\mathbf{e}_{\mathrm{I}}, \mathbf{e}_{\mathrm{II}})$ as

$$\mathbf{f} = -n_d \mu_0 \frac{\pi}{c} \left(\frac{1}{k_1^*} \left(\frac{|u|}{a} \right)^{n-1} u\mathbf{e}_1 + \frac{1}{k_2^*} \left(\frac{|v|}{a} \right)^{n-1} v\mathbf{e}_2 \right). \tag{24}$$

Three comments can be done from the last relation:

- Firstly, it is not written in an intrinsic form: its definition in another reference frame is not obvious. Within the framework presented in Section 4.1, the macroscopic flow law (24) may be written as

$$\mathbf{f} = -n_d \mu_0 \frac{\pi}{c} \left(\frac{1}{k_1^*} \left(\frac{I_{\mathrm{I}}}{a} \right)^{n-1} \mathbf{M}_{\mathrm{I}} + \frac{1}{k_2^*} \left(\frac{I_{\mathrm{II}}}{a} \right)^{n-1} \mathbf{M}_{\mathrm{II}} \right) \cdot \langle \mathbf{v}^{(0)} \rangle. \tag{25}$$

  The last equation is compatible with (22) and corresponds to the particular case where (with no summation on the indice i)

$$\varphi_i = n_d \frac{\pi}{c} \frac{\mu_0}{a^{n-1} k_i^*} I_i^{n-1}, \quad i = \mathrm{I}, \mathrm{II}. \tag{26}$$

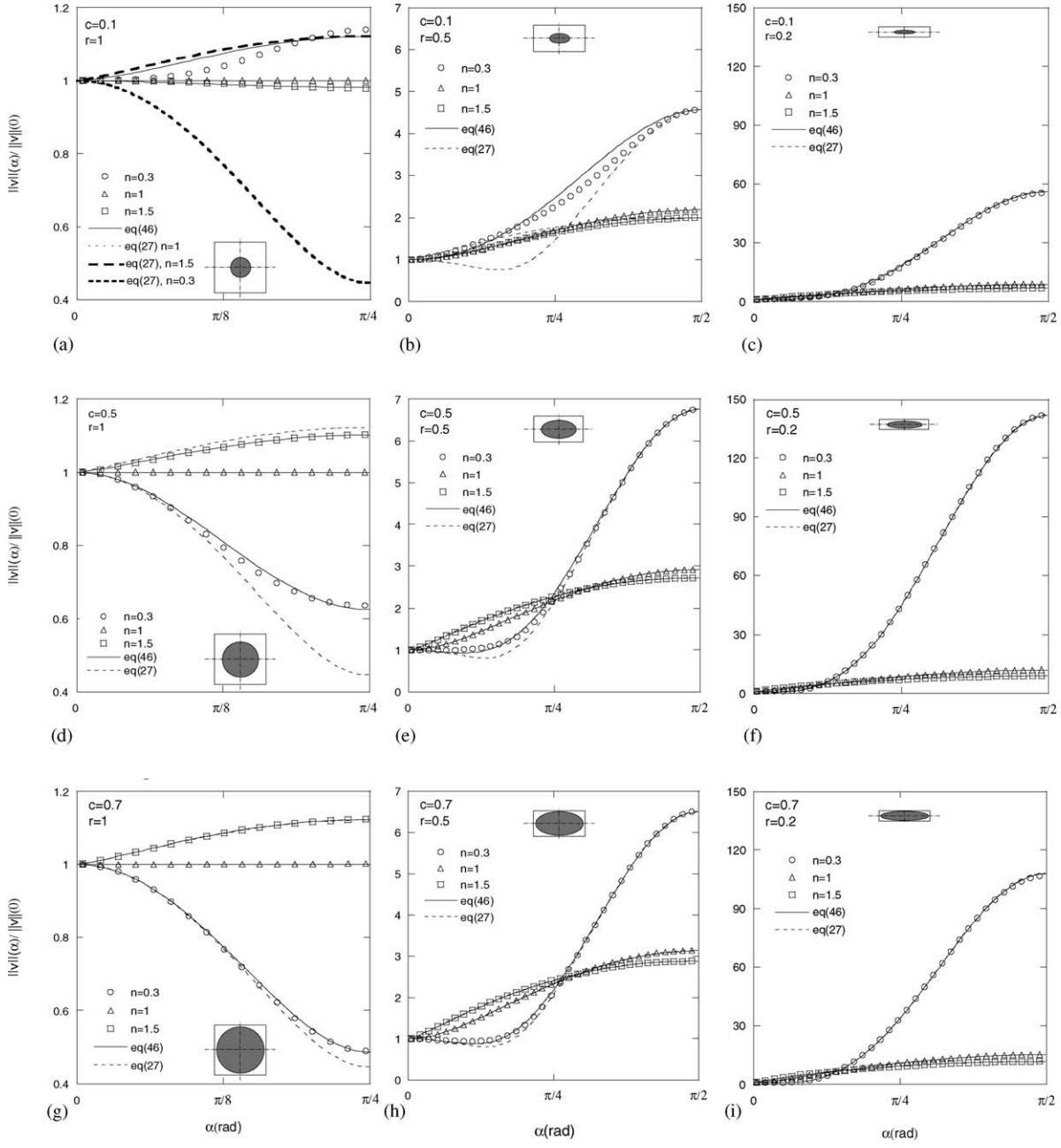

Fig. 4. Evolution of $\|\langle \boldsymbol{v}^{(0)}\rangle(\alpha)\|/\|\langle \boldsymbol{v}^{(0)}\rangle(0)\|$ as a function of α, for various power-law exponents n, for three volume fractions of fibers ($c=0.7$, 0.5 and 0.1) and for three aspect ratios ($r=1$, 0.5 and 0.2). Marks are simulation results. Dashed and continuous lines represent the prediction given by (27) and (50), respectively.

- Secondly, the flow law (24) (or (25)) implies that the norm $\|\langle \mathbf{v}^{(0)}\rangle\|$ as well as the angle β are written as ($0 \leqslant \alpha \leqslant \pi/2$)

$$\|\langle \mathbf{v}^{(0)}\rangle\| = \left(\frac{a^{n-1}}{n_d(\pi/c)\mu_0}\right)^{1/n} ((k_1^* \cos\alpha)^{2/n} + (k_2^* \sin\alpha)^{2/n})^{1/2} \|\mathbf{f}\|^{1/n}, \tag{27}$$

$$\beta = \tan^{-1}\left(\frac{k_2^*}{k_1^*}(\tan\alpha)^{1/n}\right) - \alpha. \tag{28}$$

Figs. 4 and 5 show that these relations well reproduce numerical results at volume fractions of fibers close to $c_{\max}$. A similar trend is observed when the aspect ratio deviates from 1. However, these figures also show that the differences of (28) and (27) from the simulation increase with decreasing the volume fraction of fiber or when the aspect ratio tends to 1. Indeed, because the functions φ_i in (26) only depend on I_i, the predicted flow in the $\mathbf{e}_{\mathrm{I}}$ direction is not influenced by that in the $\mathbf{e}_{\mathrm{II}}$, i.e., there is no coupling effect. When $r = 1$, Idris et al. (2004) have shown that for mild or low volume fractions of fibers, such an assumption breaks down and coupling effect between on-axis solutions should be taken into account.

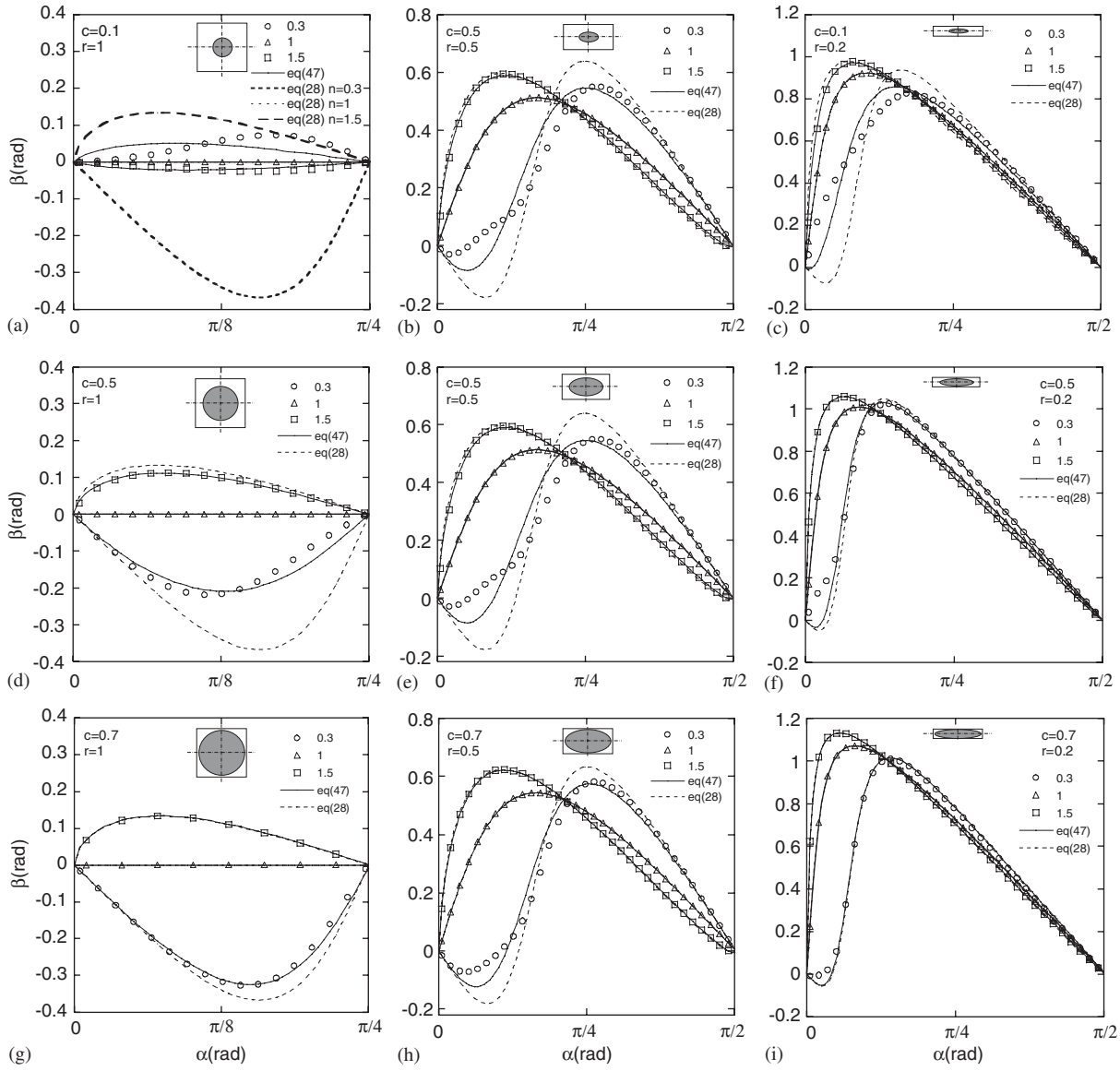

Fig. 5. Evolution of the angle β as a function of α, for various power-law exponents n, for three volume fractions of fibers ($c = 0.7$, 0.5 and 0.1) and for three aspect ratios ($r = 1$, 0.5 and 0.2). Marks are simulation results. Dashed and continuous lines represent the prediction given by (28) and (51), respectively.

- Thirdly, this law has been built for a particular type of fibrous microstructure (Fig. 1), and its application to other fibrous or porous media would require some adaptations.

4.3. A model based on iso-dissipation curves

We propose a new methodology to derive the macroscopic flow law of any given porous media. The methodology is introduced here in the case of the 2D-transverse flow through the simple fibrous microstructures depicted in Fig. 1, but its extension to 3D flow and complex microstructures is straightforward.

4.3.1. Iso-dissipation curves

Hence, the properties of the macroscopic volumetric mechanical dissipation $\mathscr{P}$ defined as

$$\mathscr{P} = -\mathbf{f}(\langle \mathbf{v}^{(0)} \rangle) \cdot \langle \mathbf{v}^{(0)} \rangle = -\nabla p^{(0)} \cdot \langle \mathbf{v}^{(0)} \rangle \tag{29}$$

is now further investigated. More precisely, mechanical iso-dissipation curves $D_{\langle \mathbf{v}^{(0)} \rangle}$ plotted in the velocity space, i.e., the loci of velocities $\langle \mathbf{v}^{(0)} \rangle$ such that the mechanical dissipation $\mathscr{P}$ is constant and equal to a given value $\mathscr{P}_0$:

$$D_{\langle \mathbf{v}^{(0)} \rangle} : \{ \langle \mathbf{v}^{(0)} \rangle | \; -\mathbf{f} \cdot \langle \mathbf{v}^{(0)} \rangle = \mathscr{P}_0 \}, \tag{30}$$

are next analyzed. They are determined from numerical results presented in Section 3.4 (subscript "§3.4"). To obtain such curves, the homogeneity of degree n of $\mathbf{f}$ with respect of $\langle \mathbf{v}^{(0)} \rangle$ is used and the positive real number ξ is determined such as

$$\begin{aligned} \mathscr{P}_0 &= \mathscr{P}(\xi \langle \mathbf{v}^{(0)} \rangle_{\S 3.4}) \\ &= -\xi^{n+1} \langle \mathbf{v}^{(0)} \rangle_{\S 3.4} \cdot \mathbf{f}_{\S 3.4} = \xi^{n+1} \mathscr{P}_{\S 3.4} \end{aligned} \tag{31}$$

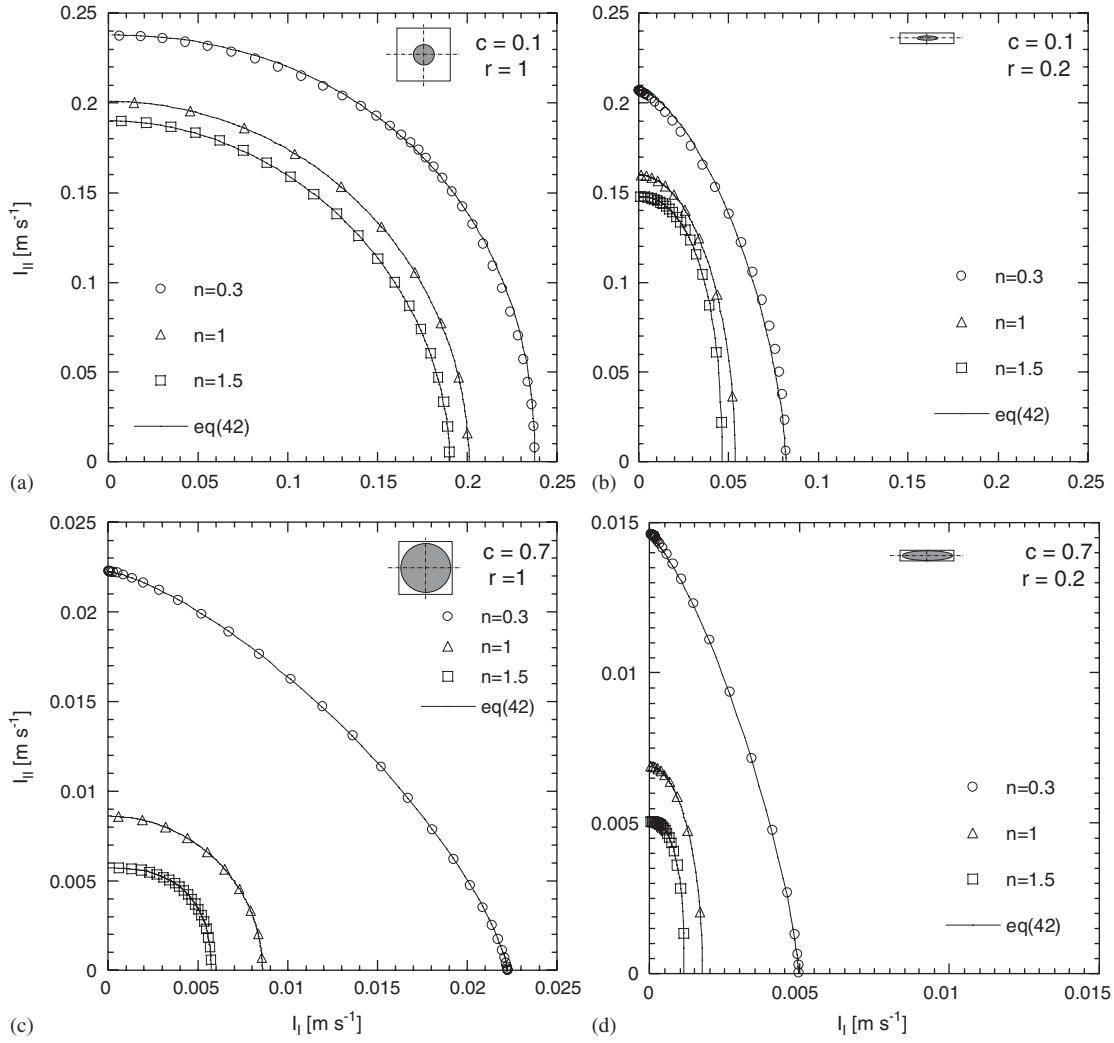

Fig. 6. Mechanical iso-dissipation curves $D_{\langle \mathbf{v}^{(0)} \rangle}$ obtained for two fiber contents ($c = 0.1$ and 0.7), $l = 1$ m, two aspects ratios ($r = 1$ and 0.2), $\mu_0 = 1\,\mathrm{Pa\,s}^n$, $\mathscr{P}_0 = 1\,\mathrm{W\,m}^{-3}$. The marks have been plotted from the simulation performed in Section 3.4 using (33). The continuous lines are the fit of (42) with the best values of m.

so that

$$\xi = \left(\frac{\mathscr{P}_0}{\mathscr{P}_{\S 3.4}} \right)^{1/(n+1)} \tag{32}$$

and

$$\langle \mathbf{v}^{(0)} \rangle = \left(\frac{\mathscr{P}_0}{\mathscr{P}_{\S 3.4}} \right)^{1/(n+1)} \langle \mathbf{v}^{(0)} \rangle_{\S 3.4} = \left(\frac{\mathscr{P}_0}{-\langle \mathbf{v}^{(0)} \rangle_{\S 3.4} \cdot \mathbf{f}_{\S 3.4}} \right)^{1/(n+1)} \langle \mathbf{v}^{(0)} \rangle_{\S 3.4}. \tag{33}$$

In the particular case of the current 2D-orthotropic microstructures, $D_{\langle \mathbf{v}^{(0)} \rangle}$ can be plotted using the $(I_\mathrm{I}, I_\mathrm{II})$ representation. This is done in Fig. 6, from which the following trends are observed:

- *when $r = 1$ and $n = 1$, iso-dissipation curves are circular* (*cf. Fig. 6(a)*): this is a direct consequence of the isotropy of the flow law in this situation.
- *when $r \neq 1$, iso-dissipation curves are stretched vertically*: as the gap $2h_2$ is smaller than $2h_1$ (cf. Fig. 1) the flow in the $\mathbf{e}_2$ direction is easier than in the $\mathbf{e}_1$ one.
- the curvature of the iso-dissipation curves depends on n, so that when n increases, the shape of the iso-dissipation seems to go from a rhomb shape for shear thinning fluids to a rectangle shape for shear thickening fluids (see Fig. 6(c)).

4.3.2. Normality rule—viscous dissipation potential

Thereby, the angle θ between the normal $\mathbf{n}$ of the mechanical iso-dissipation curve $D_{\langle \mathbf{v}^{(0)} \rangle}$ and the macroscopic volumetric viscous drag force $\mathbf{f}$ is next analyzed (see Fig. 7(a)). Within

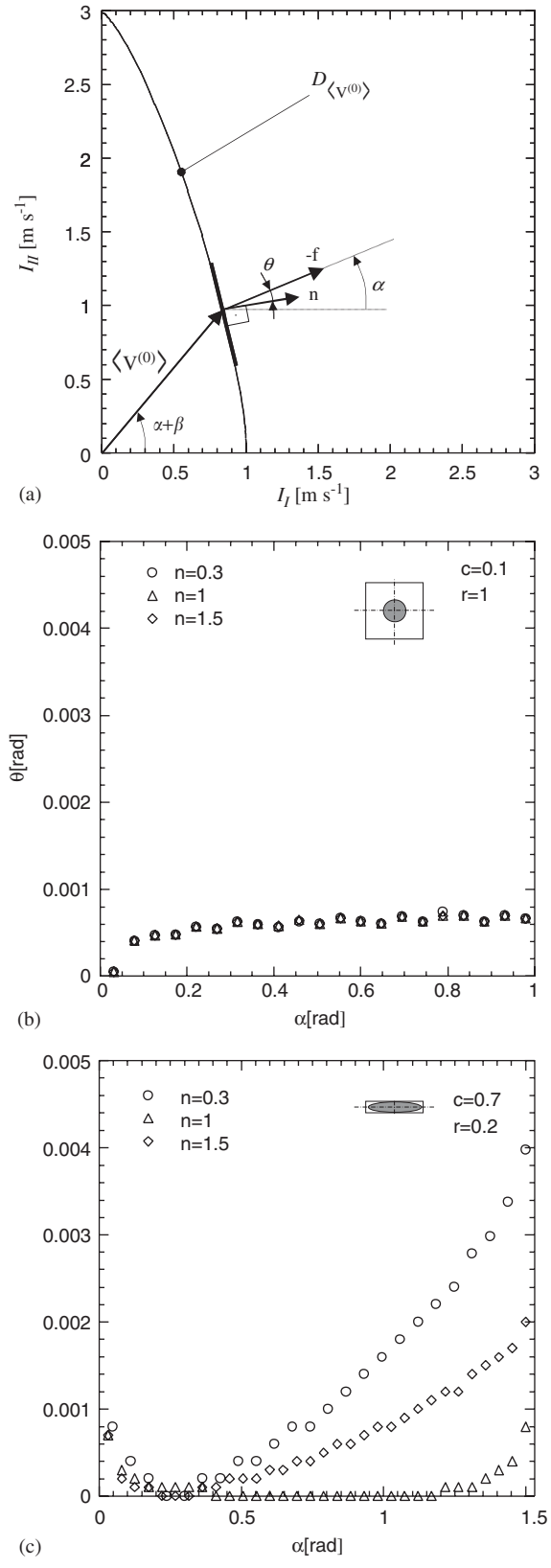

Fig. 7. (a) Definition of θ, the angle between the normal $\mathbf{n}$ to $D_{\langle \mathbf{v}^{(0)}\rangle}$ and $-\mathbf{f}$. (b) and (c) evolution of θ with the angle α for iso-dissipation curves given in Fig. 6(a) and (d), respectively.

the investigated fiber content and power-law exponent ranges, it is found that θ took very small values (< 0.004 rad) so that it could be considered as zero: this is illustrated in Fig. 7(b and c) for the iso-dissipation curves plotted in the cases where $c = 0.7$, $r = 0.2$ and $c = 0.1$, $r = 1$. Consequently, we can conclude that the volumetric viscous drag force $\mathbf{f}$ obeys to the normality rule. It can also be expressed as the gradient with respect to $\langle \mathbf{v}^{(0)}\rangle$ of a viscous dissipation potential $\Omega(\langle \mathbf{v}^{(0)}\rangle)$:

$$\mathbf{f} = -\frac{\partial \Omega(\langle \mathbf{v}^{(0)}\rangle)}{\partial \langle \mathbf{v}^{(0)}\rangle}, \tag{34}$$

with

$$\mathscr{P} = -\mathbf{f}(\langle \mathbf{v}^{(0)}\rangle) \cdot \langle \mathbf{v}^{(0)}\rangle = \chi \Omega(\langle \mathbf{v}^{(0)}\rangle), \tag{35}$$

χ being a positive constant. Such a property is very interesting since it is now possible to build a macroscopic flow in a simple way from the knowledge of iso-dissipation curves.

4.3.3. Equivalent seepage velocity—equivalent viscous drag force

To obtain a more interesting form of $\mathbf{f}$, it is possible to express Ω as a function of a scalar *equivalent seepage velocity* $v_{\mathrm{eq}}(\langle \mathbf{v}^{(0)}\rangle)$, i.e., a norm in the velocity space, so that the macroscopic drag force is now expressed as

$$\mathbf{f} = -\frac{\partial \Omega}{\partial v_{\mathrm{eq}}} \frac{\partial v_{\mathrm{eq}}}{\partial \langle \mathbf{v}^{(0)}\rangle} = f_{\mathrm{eq}} \frac{\partial v_{\mathrm{eq}}}{\partial \langle \mathbf{v}^{(0)}\rangle}, \tag{36}$$

where f_{eq} is the *equivalent viscous drag force* associated with v_{eq} in the sense:

$$\mathscr{P} = -\mathbf{f} \cdot \langle \mathbf{v}^{(0)}\rangle = -f_{\mathrm{eq}} v_{\mathrm{eq}}. \tag{37}$$

Accounting for the order of magnitude expression (5), we propose

$$f_{\mathrm{eq}} = -\frac{\mu_0}{l_c}\left(\frac{v_c}{l_c}\right)^n = -\frac{\mu_0}{l_c}\left(\frac{\zeta v_{\mathrm{eq}}}{l_c}\right)^n, \tag{38}$$

where ζ is a constant equal to v_c/v_{eq}. For 2D-orthotropic microstructures, v_{eq} only depends on I_{I} and I_{II}. Hence, using classical derivation rules

$$\begin{aligned}\frac{\partial v_{\mathrm{eq}}}{\partial \langle \mathbf{v}^{(0)}\rangle} &= \frac{\partial v_{\mathrm{eq}}}{\partial I_{\mathrm{I}}} \frac{\partial I_{\mathrm{I}}}{\partial \langle \mathbf{v}^{(0)}\rangle} + \frac{\partial v_{\mathrm{eq}}}{\partial I_{\mathrm{II}}} \frac{\partial I_{\mathrm{II}}}{\partial \langle \mathbf{v}^{(0)}\rangle} \\ &= \frac{1}{I_{\mathrm{I}}} \frac{\partial v_{\mathrm{eq}}}{\partial I_{\mathrm{I}}} \mathbf{M}_{\mathrm{I}} + \frac{1}{I_{\mathrm{II}}} \frac{\partial v_{\mathrm{eq}}}{\partial I_{\mathrm{II}}} \mathbf{M}_{\mathrm{II}},\end{aligned} \tag{39}$$

the macroscopic flow law can now be written as

$$\begin{aligned}\mathbf{f} = &-\frac{\zeta \mu_0}{l_c^2}\left(\frac{\zeta v_{\mathrm{eq}}}{l_c}\right)^{n-1} \\ &\times \left(\frac{v_{\mathrm{eq}}}{I_{\mathrm{I}}} \frac{\partial v_{\mathrm{eq}}}{\partial I_{\mathrm{I}}} \mathbf{M}_{\mathrm{I}} + \frac{v_{\mathrm{eq}}}{I_{\mathrm{II}}} \frac{\partial v_{\mathrm{eq}}}{\partial I_{\mathrm{II}}} \mathbf{M}_{\mathrm{II}}\right) \cdot \langle \mathbf{v}^{(0)}\rangle.\end{aligned} \tag{40}$$

The difficulty is now to find suitable expressions for l_c, ζ and v_{eq}:

(a) l_c, ζ and v_{eq} have been chosen such that when $\langle \mathbf{v}^{(0)}\rangle = u\mathbf{e}_{\mathrm{I}}$, the flow law (40) equals the 1D model (18), and when

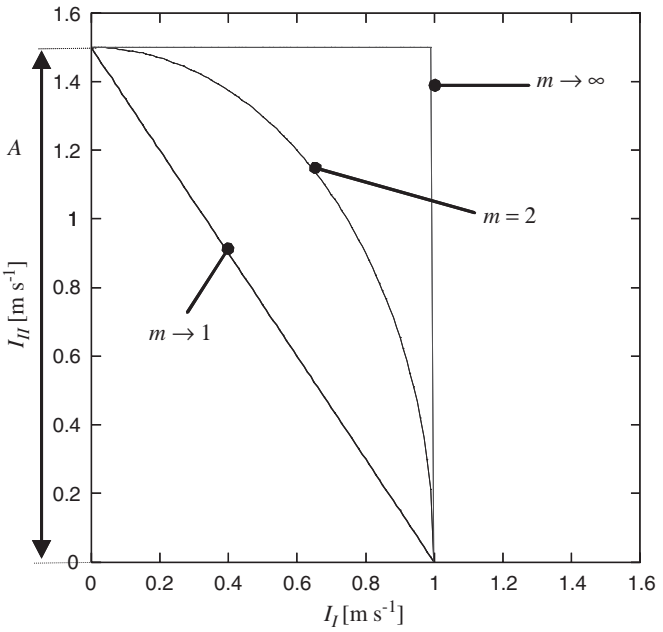

Fig. 8. Various shapes taken by iso-dissipation curves defined by (42) and plotted in the (I_{I}, I_{II}) space (in this work $I_{\mathrm{I}} = |u|$ and $I_{\mathrm{II}} = |v|$).

$\langle \mathbf{v}^{(0)} \rangle = v\mathbf{e}_{\mathrm{II}}$, (40) equals the 1D model (19). Therefore, in the particular case of the studied microstructure, l_c is directly given by (16) and ζ is deduced from (16) and (17):

$$\zeta = \frac{1}{\lambda_1(1-\sqrt{\Phi})}, \tag{41}$$

where the function λ_1 has been determined numerically in Section 3.3 (cf. Fig. 3).

(b) Then, by considering the shape of mechanical iso-dissipation curves obtained with the studied orthotropic ($r \neq 1$) and tetratropic ($r = 1$) fibrous microstructures, v_{eq} can take the following form:

$$v_{\mathrm{eq}}^m = I_{\mathrm{I}}^m + \left(\frac{I_{\mathrm{II}}}{A}\right)^m, \tag{42}$$

where $A > 0$ characterizes the anisotropy of the flow between the two symmetry axes, and $m \in]1;\infty[$ is used to modify the curvature of the iso-dissipation curve (see Fig. 8). The conditions stated in (a) as well as the expression (42) of v_{eq} imply:

$$A = \frac{1}{r}\left(\frac{\lambda_2(c,n,r)}{\lambda_1(c,n,r)}\right)^{(2n+1)/(n+1)} = \frac{1}{r}\left(\frac{\lambda_1(c,n,r^{-1})}{\lambda_1(c,n,r)}\right)^{(2n+1)/(n+1)}. \tag{43}$$

Let us remark that $A = 1$ if $r = 1$.

Accounting for the last two points, the flow law is now written

$$\mathbf{f} = -\frac{\mu_0(\sqrt{\Phi}/ra)^{n+1} v_{\mathrm{eq}}^{n-1}}{(\lambda_1(1-\sqrt{\Phi}))^{2n+1}} \times \left(\left(\frac{I_{\mathrm{I}}}{v_{\mathrm{eq}}}\right)^{m-2}\mathbf{M}_{\mathrm{I}} + \frac{1}{A^m}\left(\frac{I_{\mathrm{II}}}{v_{\mathrm{eq}}}\right)^{m-2}\mathbf{M}_{\mathrm{II}}\right)\cdot\langle\mathbf{v}^{(0)}\rangle, \tag{44}$$

v_{eq} and A being defined in (42) and (43), respectively. Notice that Eq. (44) is also compatible with (22) and that the corresponding functions φ_i now depend on both I_{I} and I_{II}

$$\varphi_i = -\frac{\mu_0(\sqrt{\Phi}/ra)^{n+1}}{(\lambda_1(1-\sqrt{\Phi}))^{2n+1}} v_{\mathrm{eq}}^{n-m+1} I_i^{m-2}, \quad i = \mathrm{I}, \mathrm{II}. \tag{45}$$

Coupling effects between flows in the $\mathbf{e}_1$ direction and the $\mathbf{e}_2$ direction are ensured through the definition of v_{eq}. Please remark that such a coupling vanishes if $m = (n+1)$: in this situation, the flow laws (44) and (25) are equivalent.

Following the same procedure and using (37) and (7b), it can be shown that the macroscopic flow law (44) can be put in the following reverse form:

$$\langle\mathbf{v}^{(0)}\rangle = -\left(\frac{(\lambda_1(1-\sqrt{\Phi}))^{2n+1}}{\mu_0(\sqrt{\Phi}/ra)^{n+1}}\right)^{1/n} f_{\mathrm{eq}}^{(1/n)-1} \times \left(\left(\frac{J_{\mathrm{I}}}{f_{\mathrm{eq}}}\right)^{M-2}\mathbf{M}_{\mathrm{I}} + A^M\left(\frac{J_{\mathrm{II}}}{f_{\mathrm{eq}}}\right)^{M-2}\mathbf{M}_{\mathrm{II}}\right)\cdot\mathbf{f}, \tag{46}$$

where $\mathbf{f} = \nabla p^{(0)}$ (according to Eq. (7b)), $M = m/(m-1)$,

$$J_i = \sqrt{\mathbf{f}\cdot\mathbf{M}_i\cdot\mathbf{f}}, \quad i = \mathrm{I}, \mathrm{II} \tag{47}$$

and where

$$f_{\mathrm{eq}}^M = J_{\mathrm{I}}^M + (AJ_{\mathrm{II}})^M. \tag{48}$$

From the upscaling process, it is shown that when $n = 1$, the macroscopic flow law (44) and the macroscopic volumetric dissipation (29) must be linear and quadratic function of $\langle\mathbf{v}^{(0)}\rangle$, respectively (Auriault, 1991). In order to fulfill this condition, the constitutive parameter m must equal 2 when $n = 1$. In this situation, the macroscopic flow law reduces to the well-known generalized Darcy's law. For the microstructures under consideration we get

$$\langle\mathbf{v}^{(0)}\rangle = -\frac{(\lambda_1(1-\sqrt{\Phi}))^3}{\mu_0(\sqrt{\Phi}/ra)^2}(\mathbf{M}_{\mathrm{I}} + A^2\mathbf{M}_{\mathrm{II}})\cdot\nabla p^{(0)}. \tag{49}$$

Also note that in the particular cases where $r = 1$ and $n = 1$, v_{eq} and f_{eq} simplify to the Euclidian norms $\|\langle\mathbf{v}^{(0)}\rangle\|$ and $\|\nabla p^{(0)}\|$, respectively.

Let us now investigate the values of the parameter m when $n \neq 1$. These values were determined by fitting Eq. (42) with the numerical iso-dissipation curves (see Fig. 6). The corresponding values of m are presented in Fig. 9. In general, m is not constant and depends on the fiber content c, the aspect ratio r and on the power-law exponent n. Anyhow, when c tends to $c_{\max}$ or r tends to ∞, then m tends to $(n+1)$. Such a tendency

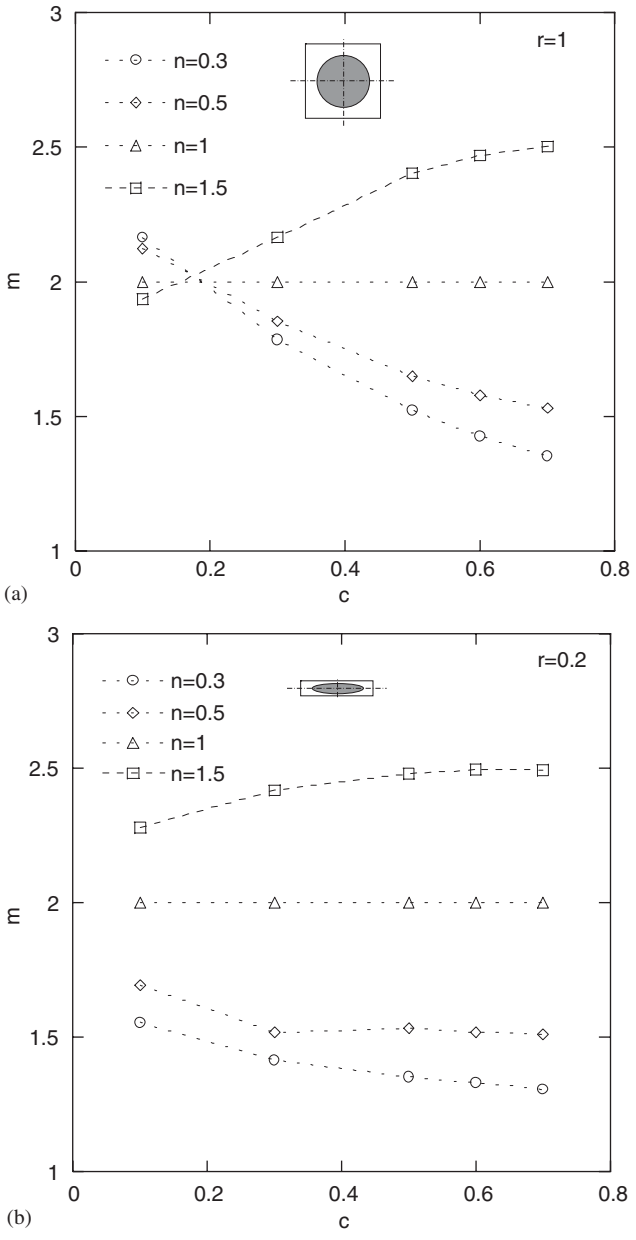

Fig. 9. Evolution of the parameter m as a function of c, for various power-law exponents n and for $r = 1$ and 0.2.

proves that the model proposed by Woods et al. (2003), i.e., (25), and the new model (44) are equivalent at fiber contents close to $c_{\max}$ or elongated cross sections.

To check the improvement brought by the new model, the predicted values of $\|\langle \mathbf{v}^{(0)} \rangle\|$ and β have been plotted in Figs. 4 and 5, respectively. Their respective expression are $(0 \leqslant \alpha \leqslant \pi/2)$:

$$\|\langle \mathbf{v}^{(0)} \rangle\| = \left(\frac{(\lambda_1(1-\sqrt{\Phi}))^{2n+1}}{\mu_0(\sqrt{\Phi}/ra)^{n+1}} \right)^{1/n} \times ((\cos\alpha)^M + (A\sin\alpha)^M)^{(1-M+1/n)/M} \times ((\cos\alpha)^{2M-2} + A^{2M}(\sin\alpha)^{2M-2})^{1/2}, \quad (50)$$

and

$$\beta = \tan^{-1}(A^M(\tan\alpha)^{M-1}) - \alpha. \quad (51)$$

These figures show that the new formulation allows a better modelling of the numerical results in the whole ranges of volume fractions of fibers, aspect ratios and power-law exponents.

5. Conclusion

The results deduced from the homogenization method for periodic structures with multiple scale expansions have been used to investigate numerically the flow of power-law fluids through anisotropic porous media. In this paper, numerical results obtained on 2D periodic arrays of parallel fibers with elliptical cross section were presented. These results clearly show the role of the volume fraction of fibers, the aspect ratio of their cross section and the fluid rheology on the resulting macroscopic flow law. In the case of on-axis flows, a simple semi-analytical expression of the 1D-flow law was proposed. This expression highlights the role of the different microstructural parameters and the fluid rheology. In order to quantify the anisotropy of the flow induced by the microstructures, the off-axis flow was then investigated. The predictions of the macroscopic model proposed by Woods et al. (2003) were compared to our numerical data. It was shown that this model allows a good description of the numerical results when the volume fraction of fibers is large and the cross section of the fibers is elongated. However, its was also shown that this model fails in reproducing our numerical data in other situations. Consequently, a new macroscopic flow law was proposed in the framework of the theory of anisotropic tensor functions and using mechanical iso-dissipation curves. This model allows a better description of the numerical results in the whole range of volume fractions of fibers, cross section aspect ratios and power-law exponents that have been investigated. Compared to the model of Woods et al. (2003), it requires only one additional constitutive parameter, which can be easily determined from the iso-dissipation curves. The methodology (theory of anisotropic tensor functions, mechanical iso-dissipation curves) presented in this paper in order to formulate the macroscopic flow law can be applied to more complex media without difficulty. Lastly, let us remark that the iso-dissipation curves can be deduced from numerical simulations on REV elementary volume but also from filtration experiments with different orientations of the pressure gradient with respect to the microstructure.

References

Advani, S.G., Bruschke, M.V., Parnas, R.S., 1994. In: Resin transfer molding flow phenomena in polymeric composites. Flow and Rheology in Polymer Composites Manufacturing.Elsevier Science, Amsterdam, pp. 465–515 (Chapter 12).

Auriault, J.L., 1991. Heterogeneous medium—is an equivalent description possible? International Journal of Engineering Science 29, 785–795.

Auriault, J.-L., Royer, P., Geindreau, C., 2002. Filtration law for power law fluids in anisotropic media. International Journal of Engineering Science 40, 1151–1163.

Bensoussan, A., Lions, J.-L., Papanicolaou, G., 1978. Asymptotic Analysis for Periodic Structures. North-Holland, Amsterdam.

Berdichevsky, A.L., Cai, Z., 1993. Perform permeability predictions by self consistent method and finite element simulation. Polymer Composites 14, 132–143.

Bernard, D., Nielsen, O., Salvo, L., Cloetens, P., 2005. Permeability assessment by 3d interdentritic flow simulations on microtomography mappings of Al–Cu alloys. Material Science and Engineering A 392, 112–120.

Boehler, J.-P., 1978. Lois de comportement anisotrope des milieux continus. Journal de Mécanique 17, 153–190.

Boehler, J.-P., 1979. A simple derivation of representations of non-polynomial constitutive equations in some cases of anisotropy. ZAMM 59, 157–167.

Boelher, J.-P., 1987. Applications of Tensor Functions in Solid Mechanics, CISM Courses and Lectures. Springer, Wien, NY.

Bourgeat, A., Mikelic, A., 1996. Homogenization of a polymer through a porous medium. Nonlinear Analysis Theory Methods and Applications 26 (7), 1221–1253.

Bruschke, M., Advani, S.G., 1993. Flow of generalized newtonian fluids across a periodic array of cylinders. Journal of Rheology 37 (3), 479–498.

Chhabra, R., Comiti, J., Machac, I., 2001. Flow of non-Newtonian fluid in fixed and fluidised beds. Chemical Engineering Science 56, 1–27.

Clague, D.S., Philips, R.J., 1997. A numerical calculation of the hydraulic permeability of three dimensional disordered fibrous media. Physics of Fluids 9, 1562–1572.

Darcy, H., 1856. Les Fontaines Publiques de la Ville de Dijon. Victor Valmont, Paris.

Edwards, D.A., Shapiro, M., Yoseph, P.B., Shapira, M., 1990. The influence of Reynolds number upon the apparent permeability of spatially periodic arrays of cylinders. Physics of Fluids A 2, 45–55.

Epstein, N., Masliyah, J.H., 1972. Creeping flow through clusters of spheroids and elliptical cylinders. Chemical Engineering Journal 3, 169–175.

Fadili, A., Tardy, P.M.J., Pearson, J.R.A., 2002. A 3D filtration law for power-law fluids in heterogeneous porous media. Journal of Non-Newtonian Fluid Mechanics 106, 121–146.

Femlab, 2004. Reference manual, version 3.0. ⟨http://www.comsol.com⟩.

Happel, J., 1959. Viscous flow relative to arrays of cylinders. A.I.Ch.E. Journal 5, 174–177.

Idris, Z., Orgéas, L., Geindreau, C., Bloch, J.-F., Auriault, J.-L., 2004. Microstructural effects on the flow law of power-law fluids through fibrous media. Modelling and Simulation in Materials Science and Engineering 12, 995–1015.

Jackson, G.W., James, D.F., 1986. The permeability of fibrous porous media. Canadian Journal of Chemical Engineering 64, 364–374.

Keller, J.B., 1964. Viscous flow through a grating or lattice of cylinders. Journal of Fluid Mechanics 18 (1), 94–96.

Koponen, A., Kandhai, D., Hellen, E., Alava, M., Hoekstra, A., Kataja, M., Niskanen, N., Sloot, P., Timonen, J., 1998. Permeability of three-dimensional random fiber webs. Physical Review Letters 80 (4), 716–719.

Kuwabara, S., 1959. The forces experienced by randomly distributed parallel circular cylinders or spheres in a viscous flow at small Reynolds numbers. Journal of the Physical Society of Japan 14, 527–532.

Liu, I., 1982. On representations of anisotropic invariants. International Journal of Engineering Science 19, 1099–1109.

Sanchez-Palencia, E., 1980. Non-homogeneous Media and Vibration Theory. In: Lectures Notes in Physics, vol. 127. Springer, Berlin.

Sangani, A., Yao, C., 1988. Transport processes in random arrays of cylinders. I. Thermal conduction. Physics of Fluids 31, 2426–2434.

Shah, C.B., Yortsos, Y., 1995. Aspect of flow of power-law fluids in porous media. A.I.Ch.E. Journal 41 (5), 1099–1112.

Smith, G., 1971. On isotropic functions of symmetric tensors skew-symmetric tensors and vectors. International Journal of Engineering Science 9, 899–916.

Song, Y., Chung, K., Kang, T., Young, J., 2004. Prediction of permeability tensor for three dimensional circular braided perform by applying a finite volume method to a unit cell. Composites Science and Technology 64, 1629–1636.

Spelt, P.D.M., Selerland, T., Lawrence, C.J., Lee, P., 2001. Drag coefficient for arrays of cylinders in flow of power-law fluids. In: Proceedings of the 14th Australian Fluid Mechanics Conference, Adelaide University.Adelaide, Australia, pp. 881–884.

Vijaysri, M., Chhabra, R.P., Eswaran, V., 1999. Power-law fluid flow across an array of infinite circular cylinders: a numerical study. Journal of Non-Newtonian Fluid Mechanics 87, 263–282.

Woods, J.K., Spelt, P.D.M., Lee, P.D., Selerland, T., Lawrence, C.J., 2003. Creeping flows of power-law fluids through periodic arrays of elliptical cylinders. Journal of Non-Newtonian Fluid Mechanics 111, 211–228.